HHS Public Access

Author manuscript

Nat Biomed Eng. Author manuscript; available in PMC 2018 October 23.

Published in final edited form as:

Nat Biomed Eng. 2018 May ; 2(5): 293–303. doi:10.1038/s41551-018-0229-7.

Cardiac recovery via extended cell-free delivery of extracellular vesicles secreted by cardiomyocytes derived from induced pluripotent stem cells

Bohao Liu[1,3,*], **Benjamin W. Lee**[1,2,*], **Koki Nakanishi**[3], **Aranzazu Villasante**[2], **Rebecca Williamson**[2,4], **Jordan Metz**[2,5], **Jinho Kim**[2], **Mariko Kanai**[3], **Lynn Bi**[2], **Kristy Brown**[4], **Gilbert Di Paolo**[4], **Shunichi Homma**[3], **Peter A. Sims**[5,6], **Veli K. Topkara**[3], and **Gordana Vunjak-Novakovic**[2,3,#]

[1]College of Physicians and Surgeons, Columbia University, New York, NY 10032

[2]Department of Biomedical Engineering, Columbia University, New York, NY 10027

[3]Department of Medicine, Columbia University, New York, NY 10032

[4]Department of Pathology and Cell Biology, Columbia University, New York, NY 10032

[5]Department of Systems Biology, Columbia University, New York, NY 10032

[6]Department of Biochemistry & Molecular Biophysics, Columbia University, New York, NY 10032

Abstract

The ability of extracellular vesicles (EVs) to regulate a broad range of cellular processes has recently been exploited for the treatment of diseases. For example, EVs secreted by stem cells injected into infarcted hearts can induce recovery through the delivery of stem-cell-specific miRNAs. However, the retention of the EVs and the therapeutic effects are short-lived. Here, we show that an engineered hydrogel patch capable of slowly releasing EVs secreted from cardiomyocytes derived from induced pluripotent stem (iPS) cells reduced arrhythmic burden, promoted ejection-fraction recovery, decreased cardiomyocyte apoptosis 24 hours after infarction, and reduced infarct size and cell hypertrophy 4 weeks post-infarction when implanted onto infarcted rat hearts. We also show that the EVs are enriched with cardiac-specific miRNAs known to modulate cardiomyocyte-specific processes. The extended delivery of EVs secreted from iPS-cell-derived cardiomyocytes into the heart may help understand heart recovery and treat heart injury.

[#]Corresponding author: Gordana Vunjak-Novakovic, University Professor, Mikati Foundation Professor of Biomedical Engineering and Medical Sciences, Columbia University, 622 West 168th Street, VC12-234, New York NY 10032, Tel: 212 305 2304, Fax: 212-305-4692, gv2131@columbia.edu, http://orion.bme.columbia.edu/gvnweb/, http://bme.columbia.edu/gordana-vunjak-novakovic.

[*]These authors contributed equally.

Competing interests statement

The authors declare no competing interests.

Author Contributions

B.L., B.W.L., G.D.P., S.H., P.A.S., V.K.T., G.V.N. designed the study. B.L., B.W.L., K.N., A.V., R.W., J.K., M.K., L.B., K.B. performed the experiments. B.L., B.W.L., J.M., analyzed the data. B.L., B.W.L., P.A.S., V.K.T., G.V.N. wrote the manuscript.

The cellular secretome represents a fundamental means of intercellular communications. This complex network of proteins, lipids, and nucleic acids allows for the regulation of a broad range of cellular behaviors and physiological functions[1]. Recently, the unique properties of the cell secretome have begun to be used as treatments in a variety of disease states[2,3]. Extracellular vesicles (EVs) are secreted microvesicles that represent an active element of the cell secretome[4–6]. In contrast to individual secreted factors, extracellular vesicles provide a unique method for cells to deliver a packaged set of bioactive components[7]. A major contributor to the activity of EVs is the collection of micro-RNAs (miRNAs) in their cargo[8]. These miRNAs are critical because they can individually modulate multiple different processes leading to pleiotropic effects[9]. Importantly, EVs from different cell types or cells in different states can carry vastly different sets of miRNAs, leading to a variety of effects[7,10]. Recent research efforts have focused on leveraging EVs as a powerful therapeutic tool.

In the treatment of heart disease, standard therapies fail to recover the injured myocardium, and do not alleviate the need for heart transplantation. Stem cell therapies of the heart demonstrated only modest improvements in ejection fraction and clinical outcomes[11–13]. While the primary use of stem cells was to form de-novo cardiomyocytes[14], their clinical benefits despite poor retention[15] have led to the discovery that implanted stem cells exert their clinical benefit largely via their secretome[12,16,17]. In particular, EVs secreted from cardiospheres or embryonic stem cells injected into the infarcted hearts were shown to attenuate ischemic injury in both small and large animal models[18–21]. Injected EVs are thought to signal directly to the myocardium and the supporting cells including fibroblasts and endothelial cells, altering their responses to ischemic injury. However, published studies have only utilized EVs from undifferentiated or partially differentiated cells, which may lack the distinct miRNAs important in cardiac-specific processes. Furthermore, similar to the key limitation of cell-based therapies, EV-based therapies of the heart relied on injections that result in short-lived retention of the EVs. To date, no group has documented EV retention greater than 3 hours post-myocardial injection[18]

Induced pluripotent stem cell derived cardiomyocytes (iCMs) offer a virtually unlimited supply of beating human cardiomyocytes. Already, there has been some success in the direct application of iCMs onto the injured myocardium including in non-human primates[22]. The clinical utility of iCMs is believed to be related to cellular engraftment onto the host myocardium and remuscularization of the infarct bed[23]. However, the presence iCMs in vivo raises concerns of tumorigenicity from undifferentiated cell fractions[12,24] and arrhythmogenicity from ectopic foci of contraction[25–27]. Previous studies using rodent neonatal cardiomyocytes have demonstrated that, similar to other cell types including stem cells, cardiomyocytes have an active secretome and can generate an abundance of EVs capable of regulating the phenotype of many target cells, including fibroblasts, endothelial cells, and other cardiomyocytes[10,28–31]. Cardiomyocyte EVs may be packaged with miRNAs with specific activity on the heart and cardiac processes. Therefore, the secretome of iCMs may contribute to their clinical effects, but has neither been characterized nor utilized therapeutically.

We hypothesized that iCMs, unlike naïve induced pluripotent stem (iPS) cells, secrete EVs carrying cardiomyocyte specific cargo that can target the myocardium both by providing protection from injury and by promoting recovery after injury (Fig 1). We also hypothesized that hydrogel encapsulation will allow for the sustained delivery of iCM EVs in the post infarct environment, promoting their therapeutic effects. To this end, we developed a system that can sustainably deliver EVs to the post infarct environment. Our results demonstrate that EVs isolated from iCMs contained a distinct set of miRNAs enriched for those known to modulate cardiomyocytes-specific processes. When encapsulated into an extended release hydrogel patch capable of delivering EVs directly to an infarcted rat heart, iCM EVs resulted in the recovery of ejection fraction, reduced infarct size, decreased arrhythmias and prevented cardiomyocyte hypertrophy. Overall, the extended delivery of iCM EVs attenuated injury and promoted recovery of the heart after ischemic insult, suggesting that iCM EVs may represent a cell-free system for understanding heart recovery and treating heart injury.

Results

iCMs secrete functional extracellular vesicles

Secreted microvesicles were isolated from iCMs and their parent iPS cells. Nanoparticle tracking analysis and visualization by transmission electron microscopy revealed that vesicles secreted by iCMs and iPS cells were comparable in yield and size, displaying typical EV morphology and size distributions[32–35] (Fig 2a–c). Immunoblots confirmed the presence of the EV marker Tumor susceptibility gene 101 (TSG101) in isolated iCM microvesicles and the absence of cell specific markers Golgin A2 (GM130) and Ras-related protein 5 (Rab5)[4] (Fig 2d, Supp Fig 7). Bioanalyzer analysis demonstrated distinct 18S and 28S rRNA peaks exclusively in iCM RNA and not in isolated iCM-EV RNA, further verifying the successful isolation of EVs without cellular contamination (Fig 2e).

To determine the ability of iCM-EVs to convey biological messages, we first confirmed the uptake of iCM-EVs by cardiac and vascular cells. iCMs and human umbilical vein endothelial cells (HUVEC) were cultured with iCM-EVs labeled with the nonspecific membrane dye DiI. Fluorescence imaging revealed EVs within both cell types (Supp Fig 1a–b). Furthermore, there was reduced iCM-EV uptake with the inhibition of dynamin-mediated endocytosis with Dynasore, but not with the inhibition of micropinocytosis with ethylisopropyl amiloride (EIPA) (Supp Fig 1c–d).

iCM-EVs have greater therapeutic potential than iPS-EVs in vitro

To compare the therapeutic potential of iPS and iCM EVs, we tested their abilities to protect iCMs in an in vitro culture model of myocardial hypoxia. Under normoxic conditions, iCMs exhibited spontaneous rhythmic contractions that became irregular after 48 hours of hypoxia (Fig 2f). Interestingly, both iPS and iCM EVs protected iCMs when added during hypoxia, reducing the range and variance of instantaneous beating frequencies. However, only iCM-EV treatment completely ameliorated the hypoxia induced phenotype (Fig 2g–h). Furthermore, iCM-EVs protected vascular cells, promoting vascular network formation during hypoxic culture (Supp Fig 2). Together, these results show that while both iCMs and

iPS cells secrete functionally active extracellular vesicles, iCM-EVs have a greater protective effect on hypoxia stressed iCMs.

iCM-EVs are enriched in cardiac specific miRNAs

To characterize in detail the miRNA cargo of extracellular vesicles, we performed next generation miRNA sequencing of iPS and iCM EVs. Sequencing results identified over 300 miRNAs with counts greater than 1 tag per million (TPM) across both groups (Supp Table 1). Dimension reduction using principal component analysis (PCA) was used to explore the broad miRNA differences between iPS and iCM EVs. This unbiased approach detected two different EV populations clearly separating iPS and iCM EVs (Fig 3a).

Next, we used DESeq2 to identify differentially expressed miRNAs between iPS and iCM EVs[36]. A total of 219 miRNAs were identified to be significantly differentially expressed with FDR values less than 0.05 (Supp Table 2). The expression levels of the subset of differentially expressed miRNAs were confirmed via quantitative real-time PCR (Supp Fig 3). Remarkably, we noted that the cardiac specific miR-1 was highly abundant in iCM-EVs but nearly absent in iPS-EVs[37]. In contrast, the early embryogenesis specific miR-302a was highly abundant in iPS-EVs and significantly decreased in iCM-EVs[38] (Table 1). A volcano plot of differentially expressed genes demonstrates asymmetric enrichment of specific miRNAs in iCM-EVs reflecting the increased miRNA diversity in iCM-EVs (Fig 3c). Interestingly, many of these miRNAs including miR-1 and miR133a are known to have significant impacts on cardiac function[39].

To predict cellular processes affected by iCM-EVs, we used miRSearch[40,41] to map the targets of a subset miRNAs that were significantly differentially expressed and highly abundant in iCM-EVs (Fig 3d, highlight). A total of 2357 genes were identified as targets (Supp Table 3). We applied gene ontology analysis to this gene set in order to identify significantly enriched biological processes[42,43], and detected 172 processes that were significantly enriched (Supp Table 4). Surprisingly, 55% of the top 20 significantly enriched biological processes with the highest fold changes are known to be heavily involved in cardiac biology (Fig 3e). Furthermore, the top 2 biological processes are those involved in the positive regulation of muscle hypertrophy. As miRNAs typically repress target function, this finding suggests that a main effect of iCM-EVs may be the repression of cardiac hypertrophy. Taken together, these results reveal that iCM-EVs contain cargo enriched in cardiac specific miRNAs that may target the hypertrophic process.

Hydrogel patch sustainably released encapsulated EVs in a rat model of acute myocardial infarction

To investigate the effects of iCM-EV treatment on heart injury and recovery, we developed a hydrogel patch capable of sustained delivery of EVs, by encapsulating approximately $3x10^{10}$ iCM-EVs into a 7mm diameter collagen gel-foam mesh. A collagen based hydrogel was selected because of it is a well-defined neutral material with documented use in sustained delivery[44]. Quantification of the release profile using NanoSight showed that the patch could sustainably release $3x10^{10}$ EVs over the course of 21 days in vitro (Fig 4a). To confirm sustained release in vivo, we labeled iCM-EVs with the membrane dye DiI, encapsulated

them into a hydrogel patch, and applied them directly onto the rat myocardium. We next imaged explanted patches after implantation using a custom laser light sheet illumination platform (Supp Fig 4a,b). At day 4 after implantation, signal intensity was reduced compared to day 0, yet indicated that a significant portion of labeled EVs remained. By day 7 after implantation, signal intensity had markedly decreased, but remained detectable. These in vivo findings were consistent with the release profile observed in vitro (Fig 4b).

After confirming delivery of iCM-EVs, we designed a rat model of myocardial infarction by left anterior descending artery (LAD) ligation to analyze the effects of iCM-EV treatment (Fig 4c). Athymic nude rats were used to remove any possible immune mediated interactions. Patches containing iPS-EVs (iPSev-P), iCM-EVs (iCMev-P), or PBS (PBS-P) were applied directly onto the rat myocardium immediately following LAD ligation. A PBS patch group was included to isolate the effects of the EV treatments from the effects of the collagen patch. Rats treated with sustained-delivery patches were compared to sham rats that received thoracotomy but no ligation or patch and MI-only rats that received ligation but no patch. Telemetry devices were implanted for telemetric monitoring of arrhythmia during the first 7 days after LAD ligation. Echocardiography was performed at 2 and 4 weeks, and the histologic analysis was performed at the 4-week endpoint.

To demonstrate that EVs deliver cargo to the myocardium in vivo, we labeled iCM-EVs with the cell membrane linker PKH-67 and incorporated them into a patch for implantation. Fluorescent imaging of frozen sections of the rat hearts 24 hours after implantation revealed the presence of labelled EVs in myocardium (Supp Fig 4c–e). Next, we quantified the levels of EV derived miRNAs in the rat myocardium and demonstrated that rat hearts treated with EV patches had significantly increased levels of miRNAs present in high quantities in EVs (Supp Fig 4f). Together these results suggest that EVs deliver their miRNA cargo when released from a patch implanted on the myocardium.

iCM-EVs were not arrhythmogenic and promoted recovery of contractile function

To determine if EVs were arrhythmogenic, we conducted continuous ECG monitoring during the first 5 days after infarction. All LAD ligation groups showed classic ECG waveform progression following MI. LAD ligation resulted in arrhythmic events including atrioventricular block (AVB), premature ventricular contraction (PVC), ventricular tachycardia (VT), and ventricular fibrillation (VF) (Fig 5a). A significant difference was noted in the cumulative arrhythmic burden (total number of events) within the first 5 days between the sham and all LAD ligation groups, but not between iCM-EV or iPS-EV and control groups (Fig 5b, Supp Fig 5a). Rats were stressed with isoproterenol, known to cause ventricular arrhythmias, seven days following surgery. Quantification of the total arrhythmic burden following isoproterenol challenge revealed that the animals treated with patches containing iPS and in particular the iCM-EVs experienced significantly fewer arrhythmic events than those treated with PBS patches without EVs. Interestingly, PBS patch treated animals showed significantly more arrhythmic events than infarcted animals that did not receive a patch (Fig 5c, Supp Fig 5b). These results indicate that EV treatment reduced did not increase the arrhythmia burden of rats.

Echocardiogram was performed at 2 and 4 weeks after LAD ligation. At 2 weeks, compared to sham rats, all LAD ligated rats showed significantly increased diastolic and systolic diameters as well as decreased ejection fraction (Fig 5d, Supp Table 5). These measurements are consistent with cardiac dilation and reduced cardiac function following injury. Interestingly, even at the 2-week time point the iCM-EV patch treated group showed reduced cardiac dilation and better function with higher ejection fraction, when compared with iPS-EV patch, PBS patch, and no patch control groups. By 4 weeks, animals treated by a iCM-EV patches no longer exhibited significant differences in any of the measured echocardiogram parameters when compared to sham animals. Additionally, iCM-EV patch treated animals showed significantly improved parameters when compared with MI-only control animals (Fig 5e, Supp Table 5). In M-mode echo, anterior wall motion was severely blunted in MI-only rats and control patch treated rats, but retained greater motion in animals treated with iCM-EV patches (Fig 5a). Of note, neither iPS-EV or PBS patch treated animals demonstrated a recovery of function at 4 weeks. Collectively, these results show that iCM-EVs protected the hearts from declining myocardial function following LAD ligation, to recover near-normal function by 4 weeks.

EV treated hearts had reduced infarct size and pathologic hypertrophy

4 weeks after LAD ligation and patch placement, the effects of iCM-EVs on the heart's response to injury were examined histologically. Movat's pentachrome staining was used to visualize the myocardium (Fig 6a–b). Total infarct size, as measured by the percentage of fibrosis in the left ventricle, was significantly smaller in iCM-EV patch treated animals than in untreated and PBS patch treated animals (Fig 6c–d). Of note, iPS-EV patch treated animals demonstrated a modest but non-significant difference in infarct size when compared to untreated and PBS patch treated animals. As sequencing analysis suggested a specific effect of iCM-EVs on hypertrophy, we quantified rat cardiomyocyte sizes at the 4-week time point. Wheat germ agglutinin staining revealed that cardiomyocyte size was significantly smaller in iCM-EV treated hearts when compared to all other LAD ligation groups (Fig 6e–f). These results suggest that iCM-EV treatment after LAD ligation was able to prevent the expansion of the infarct area and reduce pathologic hypertrophy. Finally, we performed correlation analysis to determine the interdependence of measured endpoints including total infarct size, isoproterenol induced arrhythmias, cell size, and ejection fraction. A significant positive correlation was noted between cell size and total infarct size while a significant negative correlation was noted between ejection fraction and the total infarct size and cell size (Supp Table 6).

EV treated hearts had reduced apoptosis

iCM-EV treated hearts at 4 weeks post implant did not demonstrate significant increases in infarct size compared to hearts at 24 hours after LAD ligation, in contrast to all other LAD ligation groups (Supp Fig 6). Therefore, we hypothesized that iCM-EVs may be exerting their therapeutic effect early in the injury process, and examined the function of the heart 24 hours after LAD ligation in iCM-EV patch, iPS-EV patch, and MI-only only groups (Fig 7a). Interestingly, iCM-EV patch treated animals had greater preserved ejection fraction than either iPS-EV patch treated or untreated animals suggesting that iCM-EVs may be exerting their protective effects within the first 24 hours. To determine whether this effect may have

been mediated by a reduction in ischemia induced apoptosis, we tested the ability of both iPS and iCM-EVs to reduce apoptosis in an in vitro model of cardiomyocyte ischemia. Cardiomyocytes were treated with PBS, iPS-EVs, or iCM-EVs and subsequently subjected to 1% oxygen in a hypoxic chamber for 24 hours. Quantification of apoptosis using activated caspase 3 demonstrated that iCM-EVs were able to significantly reduce apoptosis in hypoxic cardiomyocytes. Next, we examined the amount of apoptosis in rat hearts treated with a patch containing iCM-EVs or untreated hearts at 24 hours after LAD ligation. TUNEL staining showed that rats treated with iCM-EV patches had significantly decreased areas of apoptotic cells. Together, these results suggest that one of the mechanisms through which iCM-EVs are therapeutic is their ability to prevent hypoxia-induced apoptosis in newly infarcted hearts.

Discussion

We document for the first time that the extended delivery of human iCM-EVs from a hydrogel patch protects the acutely injured heart from pathologic hypertrophy and leads to functional recovery. The use of iCM-EVs thus represents a promising cell free alternative for cardiac recovery. As EVs carry cargo representative of their origin cells, the choice of cell type is crucial in determining the therapeutic potential of secreted EVs. In this study, we demonstrate significant differences in the miRNA cargo of EVs isolated from pluripotent stem cells versus terminally differentiated cardiomyocytes. We show that iCM-EVs are enriched in miRNAs that modulate cardiac specific processes. Previous studies have implicated the ability of pluripotent stem cell EVs to affect the heart through the delivery of stem cell specific miRNAs[19,38]. However, stem cell EVs may not have cell-type specific effects. We show that iCM-EVs clearly provide more therapeutic benefit after injury than iPS-EVs when released from an extended delivery patch. iCM-EVs had greater effects on reducing infarct size, hypertrophy, and apoptosis when compared to iPS-EVs. iCM-EVs were able to affect the injured heart through more cardiomyocyte specific pathways including pathologic hypertrophy. Although additional studies will be needed to elucidate the detailed mechanisms of the individual components of iCM-EV cargo, we believe that the extended delivery of cell type specific EVs represents a promising advancement in EV-based therapies of the heart.

In this study, we used iPS derived cardiomyocytes as a source of therapeutic EVs. iPS cells and their cardiac derivatives are powerful cell sources for cardiac regeneration. While previous work has highlighted the benefits of EVs derived from non-human cells, our study demonstrates the therapeutic effectiveness of EVs from human iPS cell derived cardiomyocytes. Human iPS cells offer a flexible platform to refine EV-based therapeutics. The continued improvements in differentiation[45] and maturation[46] of these cells may result in the generation of EVs with greater therapeutic potential and cardiac specificity. iPS cells are amenable to gene editing while preserving their ability to differentiation[47], allowing for the isolation of genetically modified EVs. Such a system provides the opportunity to control precisely the contents that EVs deliver. A unique property of EVs is their ability to deliver multiple miRNAs acting synergistically on separate processes to produce therapeutic effects. Thus, the ability to tailor the miRNA profiles of iCM-EVs will allow optimization of their therapeutic benefits.

One of the limitations of the use of iCMs in the injured myocardium is the concern over arrhythmogenicity due to ectopic foci of contraction or poor engraftment onto the host myocardium[25,48] We have discovered that iCM-EVs, in contrast to their cellular counterparts, do not induce arrhythmias that were observed following implantation of stem cell derived cardiomyocytes into primate hearts[22]. Most importantly, the EVs exert many of the same effects as cardiomyocyte cell therapy, including the recovery of ejection fraction, reduction of fibrosis, and prevention of cellular hypertrophy. EVs are easy to isolate and are stable frozen over long periods of time, presenting an opportunity for off-the-shelf products that can be used in the acute setting as opposed to cells which can take months to isolate and grow. Furthermore, cell therapies can often induce unwanted host immunogenic responses and although we did not study the immunogenicity of EVs in our model, recent studies have suggested that EVs have low immunogenicity[49]. Therefore, from a process-oriented standpoint, EV based cell-free therapies have a potential to bypass many of the hurdles of direct cell therapies. In particular, iCM-EVs represent an alternative to cell therapy that may be safe and practical to implement in a clinically relevant setting.

We developed and implemented an EV encapsulation method that retains EVs in the infarct environment. While a variety of methods has been suggested for delivering cells or EVs into the heart, common techniques such as single bolus injections often result in minimal concentrations of therapeutic product in the injured area, with up to 90% of cells dying or washing away in cell injections[50]. Analysis of EV retention following injection has only been completed for up to 3 hours post injection and has already shown significant decreases in EV content[18]. Encapsulation of EVs within a natural extracellular matrix patch prevents washout and maintains the local concentrations of EVs. We show that the release of EVs from the patch over the course of weeks allows for continuous and direct treatment of the infarct area through the acute and subacute phases of MI and recovery. While injections are less invasive than patch placement, hydrogels can now be delivered into the heart by percutaneous approaches[51,52], and we envision that these strategies are applicable to EV-patch deliveries.

In summary, we have shown that the extended delivery of iCM-EVs can protect and promote recovery of the heart. Although more work is required to completely elucidate the mechanisms of iCM-EV function, EVs from iCMs represent a promising new direction for understanding heart recovery and treating heart injury.

Methods

Cell Culture and Cardiomyocyte Differentiation

Human pluripotent stem cells were cultured and differentiated based on previously published protocols. Induced pluripotent stem cells (C2A line, kindly provided by Dr. Stephen Duncan through a Material Transfer Agreement (MTA)) were cultured on 1:80 diluted growth factor reduced Matrigel (Corning, Corning, NY) in mTeSR-1 (StemCell Technologies, Vancouver, CA) supplemented with 1% penicillin/streptomycin (ThermoFisher Scientific, Waltham, MA) (iPS media) at 37°C, 21% O_2. iPS cells were passaged at 80–90% confluence using 0.5 mM EDTA (ThermoFisher Scientific, Waltham, MA) and cultured for 24 hours in iPS media supplemented with 5 μM Y-27632 (Tocris Biosciences, Bristol, UK) prior to maintenance in

iPS media. Cells were used between passages 40 and 70. Pluripotent stem cell culture was performed using serum free medium.

Differentiation into cardiomyocytes was performed using a stage-based protocol in RPMI-1640 (ThermoFisher Scientific, Waltham, MA) supplemented with 0.5 mg/mL recombinant human albumin (Sigma-Aldrich, St. Louis, MO), 213 μg/mL L-ascorbic acid 2-phosphate (Sigma-Aldrich, St. Louis, MO), and 1% penicillin/streptomycin (CM media). iPS cells were grown to 80–90% confluence and changed into CM Media supplemented with 3 μM CHIR99021 (Tocris Biosciences, Bristol, UK) for 2 days. Media was then changed to CM Media supplemented with 2 μM Wnt-C59 (Tocris Biosciences, Bristol, UK) for 2 days prior to switching to CM Media without any supplements. Contracting cells were appreciated by Day 9 after the start of differentiation. Experiments were performed using wells with >70% beating cells at Day 9–21. Cardiomyocyte differentiation was performed using serum free medium.

Human umbilical vein endothelial cells (HUVECs) were isolated from discarded post-natal and fully de-identified umbilical cords under the approved IRB protocol IRB-AAAC4839. Cells were grown in endothelial growth medium-2 (EGM-2, Lonza, Basel, Switzerland) and used between passage 6 and 9.

EV Isolation and NanoSight Analysis of Size and Yield

EVs were isolated using the miRCURY^{TM} Exosome Isolation Kit (Exiqon, Vedbaek, Denmark) according to manufacturer protocol. Briefly, 50–70% confluent iPS cells or Day 12–19 iPS-CMs were washed once with PBS and switched to fresh serum-free culture media, which was collected after 48 hours incubation and centrifuged at 10,000g for 10 minutes to remove cell debris. 400 μL exosome isolation reagent was added per 1 mL media and EVs were allowed to precipitate overnight. Precipitated EVs were spun at 10,000g for 45 minutes at 4°C gently washed twice with phosphate buffered saline (PBS, ThermoFisher Scientific, Waltham, MA) resulting in a clean pellet for downstream use. Isolated EVs were reconstituted in PBS for nanoparticle tracking analysis. Particle size distributions and yield of EVs were determined with NanoSight (Malvern, Worcestershire, UK).

Transmission Electron Microscopy

EV pellets, isolated as described above, were resuspended in 4% electron microscopy grade paraformaldehyde in sodium phosphate buffer (Electron Microscopy Sciences, Hatfield, PA). 10 μL of the EVs were placed on Formvar-carbon coated electron microscopy grids (Electron Microscopy Sciences, Hatfield, PA) for 20 minutes, after which excess solution was wicked off with a filter paper. Grids were negatively stained with a uranyl-oxalate solution consisting of a 1:1 solution of 4% uranyl acetate and 0.15M oxalic acid, adjusted to pH 7 with ammonium hydroxide (all reagents from Electron Microscopy Sciences, Hatfield, MA) for 5 minutes. Excess stain was removed using a filter paper and allowed to dry. Grids were examined with a JEOL JEM-1200 EXII transmission electron microscope (Tokyo, Japan). Images were captured with an ORCA-HR digital camera (Hamamatsu, Hamamatsu, Japan) and recorded with an AMT Image Capture Engine (Advanced Microscopy Techniques, Woburn, MA).

Western Blots

iPS cells, iCMs, and EVs isolated from these cells were washed with ice cold PBS followed by lysis in RIPA buffer (ThermoFisher Scientific, Waltham, MA) supplemented with protease and phosphatase inhibitor cocktails (Roche, Basel, Switzerland), followed by centrifugation at 16,000g for 15 minutes at 4°C. Protein concentration of both the cell lysate and EV lysate were determined by Pierce BCA Protein Assay Kit (ThermoFisher Scientific, Waltham, MA). For Western blotting, lysates were fractionated via SDS-PAGE on NuPage 4–12% BisTris gels (ThermoFisher Scientific, Waltham, MA) and transferred onto nitrocellulose membranes for immunoblotting.

Antibodies were used at the following concentrations: anti-TSG101 rabbit polyclonal antibody (1:1000, abcam, Cambridge, UK), anti-GM130 mouse monoclonal antibody (1:500, BD Transduction Laboratories, Franklin Lakes, NJ), anti-Rab5 mouse monoclonal antibody (1:1000, Synaptic Systems, Goettingen, Germany).

Quantitative Polymerase Chain Reaction

Total RNA was isolated either from cells using the miRNeasy mini kit (Qiagen, Hilden, Germany) or EV pellets using the miRCURY RNA isolation kit (Exiqon, Vedbaek, Denmark) according to the manufacturer's protocol. Samples were quantified using 2100 BioAnalyzer (Agilent Technologies, Santa Clara, CA). cDNA from cells were made using the High-Capacity cDNA Reverse Transcription Kit (Applied Biosystems, Foster City, CA), and cDNA from EVs was made using the Universal cDNA synthesis kit (Exiqon, Vedbaek, Denmark). Quantitative polymerase chain reaction (qPCR) was performed on the StepOnePlus Real-Time PCR System (Applied Biosystems, Foster City, CA) where each well contained 4 μL diluted cDNA, 5 μL SYBR Green PCR Master Mix (Applied Biosystems, Foster City, CA), and 1 μL primers (all primers from Exiqon, Vedbaek, Denmark). Data were either analyzed as C_t values or using the $\Delta\Delta C_t$ method.

EV Labeling and Uptake by the Cells

Isolated and resuspended EVs were stained with 1:100 diluted DiI (ThermoFisher Scientific, Waltham, MA), a nonspecific membrane dye, for 15 minutes at room temperature. Excess dye was removed using exosome spin columns (MW 3000, ThermoFisher Scientific, Waltham, MA) per manufacturer instructions.

For uptake studies, stained EVs from 1 mL media (approx. $6x10^9$ EVs) were cultured with iPS-CMs or HUVECs for 2 hours in 37°C, 2% O_2, 5% CO_2 either in the presence of 150 μM dynasore hydrate (Sigma-Aldrich, St. Louis, MO), 75 μM 5-(N-Ethyl-N-isopropyl)amiloride (Sigma-Aldrich, St. Louis, MO), or an equivalent amount of DMSO (Corning, Corning, NY) as a control. Cells were then washed twice with PBS, fixed with 4% paraformaldehyde (ThermoFisher Scientific, Waltham, MA), and stained as outlined below. The number of EVs present in the cells was quantified using ImageJ thresholding and normalized to the total number of nuclei (DAPI) per field. Multiple fields were quantified in each case.

Measurements of Cardiomyocyte Contractility

iCMs at Day >30 post differentiation were cultured in hypoxia (2% O_2) for 2 days as a model of myocardial ischemia either in the presence of a high concentration of EVs (approx. 1.2×10^{10} EVs) or without added EVs. At baseline prior to hypoxia culture, or after two days of culture in hypoxia, videos were captured on the Olympus IX81 (Tokyo, Japan) using a Pike Camera (Allied Vision Technologies, Exton, PA) at 60 frames per second using the SPLASSH software.[37] Videos were exported into MATLAB using a custom algorithm that allowed the user to measure absolute intensity changes in a user-defined area in a frame-by-frame manner. Averaging over the entire area yielded a trace representing total movement with paired peaks, where the first narrower peak represented contraction and a second shallower and wider peak represented relaxation. The resulting traces were thresholded and the times of each contraction were obtained. The instantaneous contraction frequency was then approximated by calculating the average frequency in overlapping 5 second windows. Inter-beat variation was quantified using two metrics: the frequency range, which denotes the maximum range of instantaneous frequencies calculated for each trace and the frequency standard deviation, which denotes the standard deviation of the instantaneous frequencies calculated for each trace.

Assessment of Endothelial Networks

HUVECs of passage 6–9 were seeded onto growth factor reduced Matrigel (Corning, Corning, NY) coated surfaces at a concentration of 5×10^4 cells/cm^2 either in the presence or absence of 1.2×10^{10} EVs in hypoxia (2% O_2) as a model of ischemia for 24 hours. After 24 hours, phase contrast images were acquired using the Olympus IX81 and the Hamamatsu C4742-95 camera. Images were traced, thresholded, and skeletonized using ImageJ. The total number of branches, total number of junctions, and cumulative network length were quantified for each skeleton.

Assessment of hypoxia-induced cardiomyocyte death

iPS-CMs at >30 days post differentiation were cultured in hypoxia (2% O_2) for 24 hours as a model of myocardial ischemia either in the presence of a high concentration of iPS-EVs, iCM-EVs (~ 1.25×10^9 EVs), or without added EVs. Cells were then washed twice with PBS, fixed with 4% paraformaldehyde (ThermoFisher Scientific, Waltham, MA), and stained as outlined below. Activated caspase 3 positive cells were quantified using ImageJ thresholding. Multiple fields were quantified for each sample.

EV miRNA Sequencing

Isolated total RNA from four iPS-EV and four iCM-EV samples were sent to Exiqon for microRNA library preparation, sequencing, and mapping. Eight separate microRNA profiles were generated. Raw counts were converted to tags per million (TPM), then visualized by principal component analysis along the first three principal components using the scikit-learn library in Python. Raw count tables for these samples were used as input to DESeq2 to determine differential expression of microRNAs between the iPS-EV and iCM-EV groups. The sets of predicted targets for each of the miRNAs with greatest differential expression and abundance in iCM-EVs were determined with Exiqon's prediction algorithm,

miRSearch. These targets were collectively analyzed with PANTHER for gene ontology enrichment.

Patch Preparation and EV Release Kinetics

EV-containing patches were created via gelation of collagen within a gelfoam mesh. Gelfoam (Pfizer, New York, NY) was cut into 7 mm diameter cylinders using a dermal biopsy punch (Miltex, Plainsboro, NJ) under sterile conditions. 100 μL of collagen/EV solution containing 2 mg/mL rat tail Collagen Type I (Corning, Corning, NY) buffered to neutral pH with 10x Dulbecco's Modified Eagle Medium, HEPES, and 1 M sodium hydroxide (ThermoFisher Scientific, Waltham, MA) and $3x10^{10}$ EVs in PBS was added to each gelfoam mesh and polymerized at 37°C for 30 minutes. This resulted in approximately 10^8 EVs per gram body weight loaded into the patch which is in line with previous animal studies[18,53]. Patches without EVs served as a control. Patches were washed once for 30 seconds in PBS and used either for characterization of EV release or immediate implantation into a rat.

For the release experiment, patches were immersed in 1 mL PBS at 37°C. PBS was replaced every two days for the first 14 days and one final time on day 21. Release was quantified by NanoSight as above. Laser light sheet fluorescence microscopy was used to image explanted EV patches at 0, 4, and 7 days after implantation. The light sheet imaging system was constructed using commercially available optical parts and hardware. A thin laser sheet (thickness: ~ 3 um) was created by passing the laser beam (Jive 561 nm 200 mW laser, Cobolt) through a cylindrical lens (ACY254-050-A, Thorlabs). A mirror (PF10-03-M01, Thorlabs) was placed between the laser source and the cylindrical lens to change the laser beam direction. The laser sheet was then illuminated across the heart patch that was placed onto a motorized sample stage (PT1-Z8, Thorlabs). The emission light from EVs within the patch were passed through an optical filter (FF02-641/75-25, Semrock) and a tube lens (U-TLU, Olympus), and imaged by a camera (Zyla sCMOS 4.2, Andor) with the 4× (PlanN 4×, NA 0.10, Olympus), 10× (PlanN 10×, NA 0.25, Olympus), and 20× (LUCPlanFLN 20×, NA 0.45, Olympus) objective lenses.

For in-vivo uptake studies, EVs from 10 mL media (approx. $3x10^{10}$ EVs) were stained with PKH-67 (Sigma-Aldrich, St Louis, MO) per manufacturer instructions. Excess dye was removed using exosome spin columns as previously described. Labelled EVs were incorporated into the collagen patch and implanted onto the rat myocardium. Rat hearts were then explanted for histological analysis.

Rat Model of Acute Myocardial Infarction

Animal work was performed under a Columbia University Institutional Animal Care and Use Committee (IACUC) approved protocol. Athymic nude (Hsd:RH-Foxn1^{rnu}) Sprague Dawley Rats (Harlan, Indianapolis, IN) age 15–19 weeks were first implanted with a bipotential telemeter (CTA-F40) capable of transmitting electrocardiogram, temperature, and movement data to a paired receiver and computer (all from Data Sciences International, St. Paul, MN). Rats were anesthetized with a cocktail of 95 mg/kg ketamine and 5 mg/kg xylazine. The CTA-F40 telemeter (Data Sciences International, St. Paul, MN) was placed in

the dorsal subcutaneous space and leads were positioned subcutaneously in a standard lead II configuration and sutured to the underlying muscle.

One week after telemeter placement, rats received a myocardial infarction (MI) by left anterior descending (LAD) artery ligation and were subsequently implanted with a patch. Rats were anesthetized with a cocktail of 95 mg/kg ketamine and 5 mg/kg xylazine, intubated, and mechanically ventilated on 100% O_2 with 1–5% inhaled isoflurane. The heart was exposed by left thoracotomy, the LAD was ligated using an 8-0 prolene suture (Covidien, Dublin, Ireland), and success of the ligation was confirmed when the anterior wall of the left ventricle turned pale. The patch was fabricated as described above, washed briefly in PBS and immediately sutured onto the myocardium using 2 8-0 sutures. Electrocardiograms were monitored for at least one week and echocardiograms were recorded several times over the one month experimental period. Rats were euthanized with CO_2 4 weeks after LAD ligation, and hearts were immediately explanted, washed twice with ice cold PBS, weighed, grossly sectioned, and prepared for histological analysis.

Telemetric Monitoring of Cardiac Function

Animals were implanted with telemetric transmitters (CTA-F40) one week prior to LAD ligation. Electrocardiograms were acquired continuously from one day prior to LAD ligation surgery to 8 days following surgery using the Data Sciences International system on Ponemah 6.0 software. At seven days following LAD ligation, rats were challenged with 0.1 mg/kg isoproterenol (Sigma-Aldrich, St. Louis, MO), known to induce ventricular arrhythmias in rats.

Raw electrocardiogram traces were viewed in Ponemah 6.0 (Data Sciences International) as follows: for five days following LAD ligation, the number of arrhythmic events (atrioventricular block, premature ventricular contraction, ventricular tachycardia, or ventricular fibrillation), were counted for one minute every ten minutes. The number of arrhythmic events was also counted continuously for the three hours following isoproterenol injection. The mean event times were calculated as the mean of the mean event times for each animal.

Echocardiography

Serial echocardiography was carried out at 2 and 4 weeks after the LAD ligation and patch placement. Rats were placed under light anesthesia (2% isoflurane) and were imaged using the SONOS 5500 system (Philips, Amsterdam, Netherlands) equipped with a S12 transducer (12-MHz). M-mode images and gray-scale two-dimensional parasternal short-axis images at the mid-papillary level were recorded in each rat. Measurements were made offline by a single observer in a group-blinded fashion. Left ventricular (LV) end-diastolic and end-systolic internal diameters were measured from M-mode images permitting calculation of LV fractional shortening (FS), LV end-diastolic volume, LV end-systolic volume, and ejection fraction (EF). Heart rates were determined using M-mode images. All parameters represent the average of 3 beats.

Histology

Hearts were fixed in 4% paraformaldehyde (ThermoFisher Scientific, Waltham, MA) for 24 hours, then subsequently placed in 70% ethanol. Samples were paraffin embedded and 5 μm thin transverse sections of the heart were obtained. Slides were deparaffinized in Citrisolv (ThermoFisher Scientific, Waltham, MA) for five minutes, and rehydrated using an ethanol gradient. Slides were stained with Movat's Pentachrome using standard procedures or antigen retrieved with citrate buffer and immunostained as below.

Immunostaining

Fixed cells or sections were washed with PBS, permeabilized with 0.1% Triton-X (Sigma-Aldrich, St. Louis, MO), and blocked with 5% bovine serum albumin (BSA, Sigma-Aldrich, St. Louis, MO) for 2 hours. Primary and secondary antibodies were applied for 1 hour each, with 3 × 10 minute PBS washes between. Antibody details are as follows: polyclonal rabbit anti-active caspase 3 (1:40, Abcam, Cambridge, MA), monoclonal mouse anti-cardiac troponin T (4 μg/mL, Developmental Studies Hybridoma Bank, Iowa City, IA, Alexa Fluor 488 goat anti-mouse IgG (1:500, ThermoFisher Scientific, Waltham, MA), Alexa Fluor 488 goat anti-rabbit IgG (1:500, ThermoFisher Scientific, Waltham, MA), Alexa Fluor 594 goat anti-mouse IgG (1:500, ThermoFisher Scientific, Waltham, MA). TUNEL staining was conducted with the in situ cell death detection kit (Sigma-Aldrich, St. Louis, MO). Cells and sections were counterstained with DAPI (ThermoFisher Scientific, Waltham, MA) or Alexa Fluor 594 conjugated Wheat Germ Agglutinin (ThermoFisher Scientific, Waltham, MA) per manufacturer protocol. Sections were mounted using ProLong Gold Antifade Mountant with DAPI (ThermoFisher Scientific, Waltham, MA). Fluorescence images were taken using the Olympus IX81 microscope (Tokyo, Japan) and the Hamamatsu C4742-95 camera (Hamamatsu, Japan). All images were post-processed and quantified using ImageJ.

Statistics and correlation analysis

Statistical testing was performed using two tailed T-test. Bonferroni correction was used to adjust for multiple corrections. Statistical significance was determined by $p<0.05$ unless otherwise stated.

Correlation analysis was conducted between each pair of total infarct size, isoproterenol induced arrhythmic events, cell size, and ejection fraction sets of measurements using Pearson correlation test.

Data Availability

The authors declare that all data supporting the findings of this study are available within the paper and its supplementary information. Source data are available from the corresponding author upon reasonable request.

Code Availability

The custom computer code used in this study is available from the corresponding author upon reasonable request.

Supplementary Material

Refer to Web version on PubMed Central for supplementary material.

Acknowledgments

We thank Dr. Malcolm Moore (Memorial Sloan-Kettering Cancer Center) for kindly making available the particle tracking instrument (NanoSight) and Dr. Srikanth R. Ambati and Dr. Ashish Saxena (Memorial Sloan-Kettering Cancer Center) for technical help. We thank Qing Li for performing animal surgeries, Rui Liu and Leonid Zaurov for assistance with animal echocardiograms, and Sue Halligan for coordinating the animal work. We thank Diogo Teles, Nathan Kim, and Adam Pluchinksky for assistance with the experiments. We thank Dr. Barry Fine for valuable discussions of the manuscript. We gratefully acknowledge funding of this work by NIH (HL076485, EB002520, EB17103, GM007367), NYSTEM (C028119), and NIA (F30 AG047748).

References

1. Stastna M, Van Eyk JE. Investigating the Secretome. Circ Cardiovasc Genet. 2012; 5
2. Wei K, et al. Epicardial FSTL1 reconstitution regenerates the adult mammalian heart. Nature. 2015; 525:479–485. [PubMed: 26375005]
3. Ohno S, et al. Systemically injected exosomes targeted to EGFR deliver antitumor microRNA to breast cancer cells. Mol Ther. 2013; 21:185–91. [PubMed: 23032975]
4. Raposo G, Stoorvogel W. Extracellular vesicles: Exosomes, microvesicles, and friends. J Cell Biol. 2013:200.
5. Tkach M, Théry C. Communication by Extracellular Vesicles: Where We Are and Where We Need to Go. Cell. 2016; 164:1226–1232. [PubMed: 26967288]
6. Lo Cicero A, Stahl PD, Raposo G. Extracellular vesicles shuffling intercellular messages: for good or for bad. Curr Opin Cell Biol. 2015; 35:69–77. [PubMed: 26001269]
7. Emanueli C, Shearn AIU, Angelini GD, Sahoo S. Exosomes and exosomal miRNAs in cardiovascular protection and repair. Vascul Pharmacol. 2015; 71:24–30. [PubMed: 25869502]
8. Stoorvogel W. Functional transfer of microRNA by exosomes. Blood. 2012:119.
9. Olson EN. MicroRNAs as therapeutic targets and biomarkers of cardiovascular disease. Sci Transl Med. 2014; 6:239ps3.
10. Malik ZA, et al. Cardiac myocyte exosomes: stability, HSP60, and proteomics. AJP Hear Circ Physiol. 2013; 304:H954–H965.
11. Stamm C, et al. Autologous bone-marrow stem-cell transplantation for myocardial regeneration. Lancet. 2003; 361:45–46. [PubMed: 12517467]
12. Garbern JC, Lee RT. Cardiac stem cell therapy and the promise of heart regeneration. Cell Stem Cell. 2013; 12:689–98. [PubMed: 23746978]
13. Segers VFM, Lee RT. Stem-cell therapy for cardiac disease. Nature. 2008; 451:937–942. [PubMed: 18288183]
14. Toma C, Pittenger MF, Cahill KS, Byrne BJ, Kessler PD. Human mesenchymal stem cells differentiate to a cardiomyocyte phenotype in the adult murine heart. Circulation. 2002; 105:93–8. [PubMed: 11772882]
15. Vrtovec B, et al. Effects of intracoronary CD34+ stem cell transplantation in nonischemic dilated cardiomyopathy patients: 5-year follow-up. Circ Res. 2013; 112:165–173. [PubMed: 23065358]
16. Karantalis V, Hare JM. Use of Mesenchymal Stem Cells for Therapy of Cardiac Disease. Circ Res. 2015; 116:1413–1430. [PubMed: 25858066]
17. Godier-Furnémont AFG, et al. Composite scaffold provides a cell delivery platform for cardiovascular repair. Proc Natl Acad Sci U S A. 2011; 108:7974–9. [PubMed: 21508321]
18. Gallet R, et al. Exosomes secreted by cardiosphere-derived cells reduce scarring, attenuate adverse remodelling, and improve function in acute and chronic porcine myocardial infarction. Eur Heart J. 2016; :ehw240.doi: 10.1093/eurheartj/ehw240

19. Khan M, et al. Embryonic Stem Cell-Derived Exosomes Promote Endogenous Repair Mechanisms and Enhance Cardiac Function Following Myocardial Infarction. Circ Res. 2015; 117:52–64. [PubMed: 25904597]
20. Bian S, et al. Extracellular vesicles derived from human bone marrow mesenchymal stem cells promote angiogenesis in a rat myocardial infarction model. J Mol Med. 2014; 92:387–397. [PubMed: 24337504]
21. Mackie AR, et al. Sonic Hedgehog-Modified Human CD34+ Cells Preserve Cardiac Function After Acute Myocardial Infarction. Circ Res. 2012; 111:312–321. [PubMed: 22581926]
22. Chong JJH, et al. Human embryonic-stem-cell-derived cardiomyocytes regenerate non-human primate hearts. 2014; doi: 10.1038/nature13233
23. Laflamme MA, et al. Cardiomyocytes derived from human embryonic stem cells in pro-survival factors enhance function of infarcted rat hearts. Nat Biotechnol. 2007; 25:1015–1024. [PubMed: 17721512]
24. Lee AS, Tang C, Rao MS, Weissman IL, Wu JC. Tumorigenicity as a clinical hurdle for pluripotent stem cell therapies. Nat Med. 2013; 19:998–1004. [PubMed: 23921754]
25. Chong JJH, et al. Human embryonic-stem-cell-derived cardiomyocytes regenerate non-human primate hearts. Nature. 2014; 510:273–277. [PubMed: 24776797]
26. Serpooshan V, Wu SM. Patching Up Broken Hearts: Cardiac Cell Therapy Gets a Bioengineered Boost. Cell Stem Cell. 2014; 15:671–673. [PubMed: 25479741]
27. Anderson ME, Goldhaber JI, Houser SR, Puceat M, Sussman MA. Embryonic Stem Cell--Derived Cardiac Myocytes Are Not Ready For Human Trials. Circ Res. 2014
28. Waldenström A, Gennebäck N, Hellman U, Ronquist G, Minetti C. Cardiomyocyte Microvesicles Contain DNA/RNA and Convey Biological Messages to Target Cells. PLoS One. 2012; 7:e34653. [PubMed: 22506041]
29. Garcia NA, Moncayo-Arlandi J, Sepulveda P, Diez-Juan A. Cardiomyocyte exosomes regulate glycolytic flux in endothelium by direct transfer of GLUT transporters and glycolytic enzymes. Cardiovasc Res. 2016; 109:397–408. [PubMed: 26609058]
30. Wang X, et al. Cardiomyocytes mediate anti-angiogenesis in type 2 diabetic rats through the exosomal transfer of miR-320 into endothelial cells. J Mol Cell Cardiol. 2014; 74:139–150. [PubMed: 24825548]
31. Zhang X, et al. Hsp20 Functions as a Novel Cardiokine in Promoting Angiogenesis via Activation of VEGFR2. PLoS One. 2012; 7:e32765. [PubMed: 22427880]
32. Kishore R, Khan M. More Than Tiny Sacks. Circ Res. 2016; 118:330–343. [PubMed: 26838317]
33. Chernyshev VS, et al. Size and shape characterization of hydrated and desiccated exosomes. Anal Bioanal Chem. 2015; 407:3285–3301. [PubMed: 25821114]
34. Mateescu B, et al. Obstacles and opportunities in the functional analysis of extracellular vesicle RNA - an ISEV position paper. J Extracell vesicles. 2017; 6:1286095. [PubMed: 28326170]
35. Witwer KW, et al. Standardization of sample collection, isolation and analysis methods in extracellular vesicle research. J Extracell Vesicles. 2013; 2:20360.
36. Love MI, Huber W, Anders S. Moderated estimation of fold change and dispersion for RNA-seq data with DESeq2. Genome Biol. 2014; 15:550. [PubMed: 25516281]
37. Yang B, et al. The muscle-specific microRNA miR-1 regulates cardiac arrhythmogenic potential by targeting GJA1 and KCNJ2. Nat Med. 2007; 13:486–491. [PubMed: 17401374]
38. Tian Y, et al. A microRNA-Hippo pathway that promotes cardiomyocyte proliferation and cardiac regeneration in mice. Sci Transl Med. 2015; 7:279ra38.
39. Carè A, et al. MicroRNA-133 controls cardiac hypertrophy.
40. Lewis BP, et al. Conserved Seed Pairing, Often Flanked by Adenosines, Indicates that Thousands of Human Genes are MicroRNA Targets. Cell. 2005; 120:15–20. [PubMed: 15652477]
41. Garcia DM, et al. Weak seed-pairing stability and high target-site abundance decrease the proficiency of lsy-6 and other microRNAs. Nat Struct Mol Biol. 2011; 18:1139–46. [PubMed: 21909094]
42. Consortium TGO. Gene Ontology Consortium: going forward. Nucleic Acids Res. 2015; 43:D1049–D1056. [PubMed: 25428369]

43. Ashburner M, et al. Gene Ontology: tool for the unification of biology. Nat Genet. 2000; 25:25–29. [PubMed: 10802651]
44. Wallace DG, Rosenblatt J. Collagen gel systems for sustained delivery and tissue engineering. Adv Drug Deliv Rev. 2003; 55:1631–49. [PubMed: 14623405]
45. Protze SI, et al. Sinoatrial node cardiomyocytes derived from human pluripotent cells function as a biological pacemaker. Nat Biotechnol. 2016; 35:56–68. [PubMed: 27941801]
46. Eng G, et al. Autonomous beating rate adaptation in human stem cell-derived cardiomyocytes. Nat Commun. 2016; 7:10312. [PubMed: 26785135]
47. Sontag S, et al. Modelling IRF8 Deficient Human Hematopoiesis and Dendritic Cell Development with Engineered iPS Cells. Stem Cells. 2017; 35:898–908. [PubMed: 28090699]
48. Chen HSV, Kim C, Mercola M. Electrophysiological Challenges of Cell-Based Myocardial Repair. Circulation. 2009; 120:2496–2508. [PubMed: 20008740]
49. Zhu X, et al. Comprehensive toxicity and immunogenicity studies reveal minimal effects in mice following sustained dosing of extracellular vesicles derived from HEK293T cells. J Extracell Vesicles. 2017; 6:1324730. [PubMed: 28717420]
50. Hou D, et al. Radiolabeled cell distribution after intramyocardial, intracoronary, and interstitial retrograde coronary venous delivery: implications for current clinical trials. Circulation. 2005; 112:I150–6. [PubMed: 16159808]
51. Seif-Naraghi SB, et al. Safety and Efficacy of an Injectable Extracellular Matrix Hydrogel for Treating Myocardial Infarction. Sci Transl Med. 2013; 5
52. Lang N, et al. A Blood-Resistant Surgical Glue for Minimally Invasive Repair of Vessels and Heart Defects. Sci Transl Med. 2014; 6
53. Ibrahim AGE, Cheng K, Marbán E. Exosomes as critical agents of cardiac regeneration triggered by cell therapy. Stem cell reports. 2014; 2:606–19. [PubMed: 24936449]

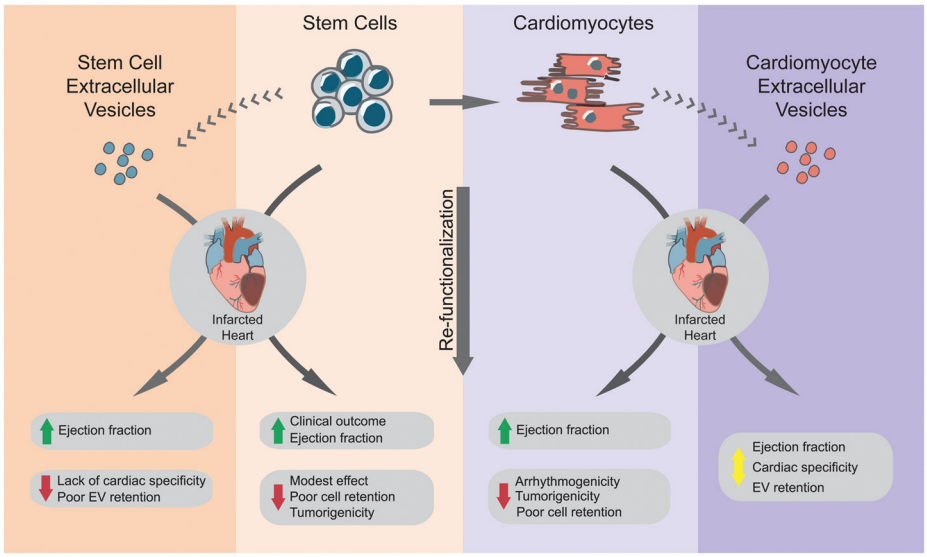

Figure 1. Therapeutic potential and challenges of cell and extracellular vesicle-based therapies

Cell based therapies utilizing either stem cells or differentiated cardiomyocytes have shown clinical utility in their ability to re-functionalize the injured heart. When directly injected into the heart, both stem cells and cardiomyocytes have resulted in the re-functionalization of the heart and improved clinical outcomes[11–13]. However, many challenges arise from the use of cell therapies. Specifically, stem cell therapies only demonstrate modest effects while cardiomyocyte therapies show high propensity of arrhythmogenicity[22,26,27]. Stem cell extracellular vesicles (EVs) have also been able to re-functionalize the injured heart, mediating the regeneration of the heart after myocardial infarction[12,16,19,20]. However, the cargo of stem cell EVs is not specific to cardiac processes. We hypothesize that iCMs, unlike naïve iPS cells, secrete EVs carrying cardiomyocyte specific cargo that can target the myocardium, providing protection from injury and promoting recovery after myocardial infarction.

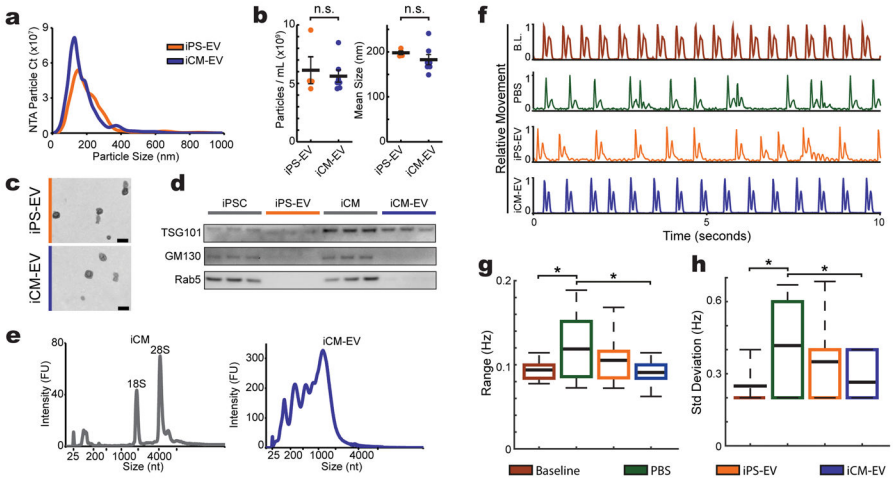

Figure 2. iCMs secrete functional EVs

a) Representative size distribution of microvesicles isolated from iPS cells and iCMs. b) Total number and size of microvesicles (Average ± SEM, n = 4 and 8 biologically independent samples for iPS and iCM groups respectively). c) Representative transmission electron micrographs of microvesicles (scale = 100 nm, experiments were repeated with similar results). d) Immunoblots of cell lysates and microvesicle fractions for the exosome marker TSG101, and intracellular proteins (GM130, Rab5) (n = 3 biologically independent samples per group). e) Representative bioanalyzer plots of total RNA profiles of iCMs and iCM-EVs (n = 3 biologically independent samples per group). f) Representative traces of spontaneously beating iCMs at baseline (normoxia) and after 48 hours of hypoxia, without EVs, and with iPS or iCM-EVs (experiments were repeated with similar results). Range (g) and standard deviation (h) of the distributions of instantaneous beating frequencies. Boxes show mean, 25th and 75th percentiles. Whiskers show 9th to 91st percentile. (n = 49, 35, 12, and 31 biologically independent samples for baseline, PBS, iPS-Ev, and iCM-Ev groups respectively, * denotes $p < 0.05$ by two sided T-test).

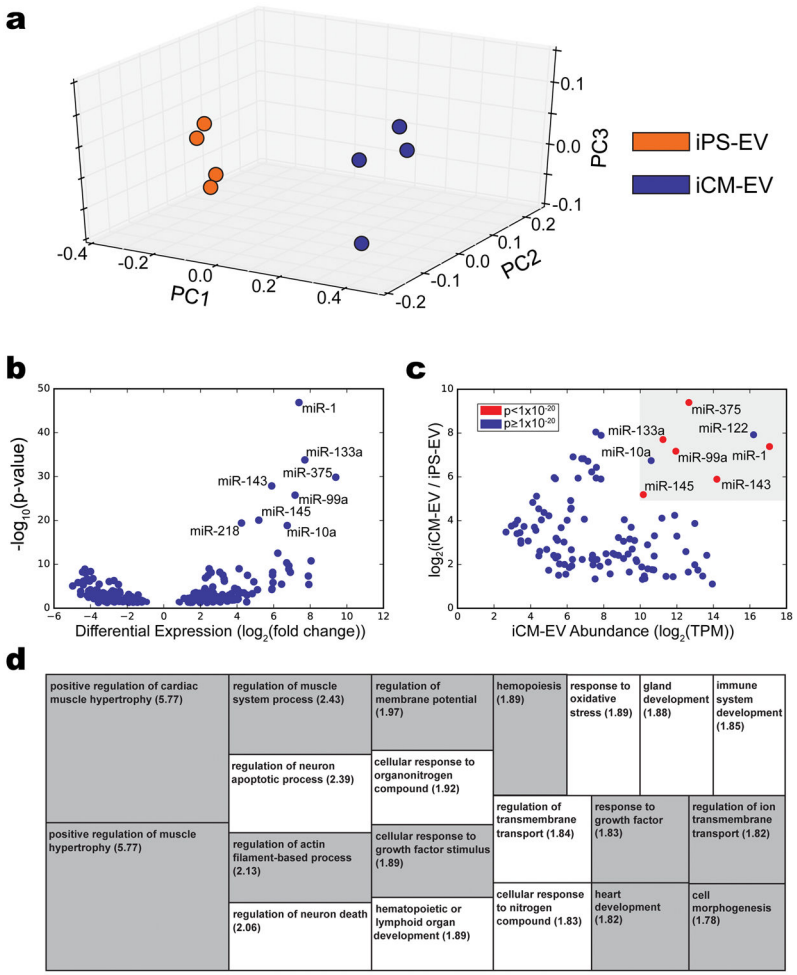

Figure 3. iCM-EVs are enriched in cardiac specific miRNAs

a) Principal component analysis of iPS-EV and iCM-EV miRNA expression (n = 4 biologically independent samples per group). b) Fold change and expression levels (Tags per million) of the most abundant miRNAs in iCM-EVs that are differentially expressed. c) Volcano plot of significantly differentially expressed miRNAs. P-values calculated via Wald test and adjusted with the Benjamini-Hochberg method (n = 4 biologically independent samples per group). d) Differentially expressed and abundantly expressed miRNAs in iCM-EVs. Highlighted region contains miRNAs used in subsequent gene ontology analysis. (n = 4 biologically independent samples per group). Fold change over expected enrichment shown in parenthesis; cardiac related processes highlighted in gray.

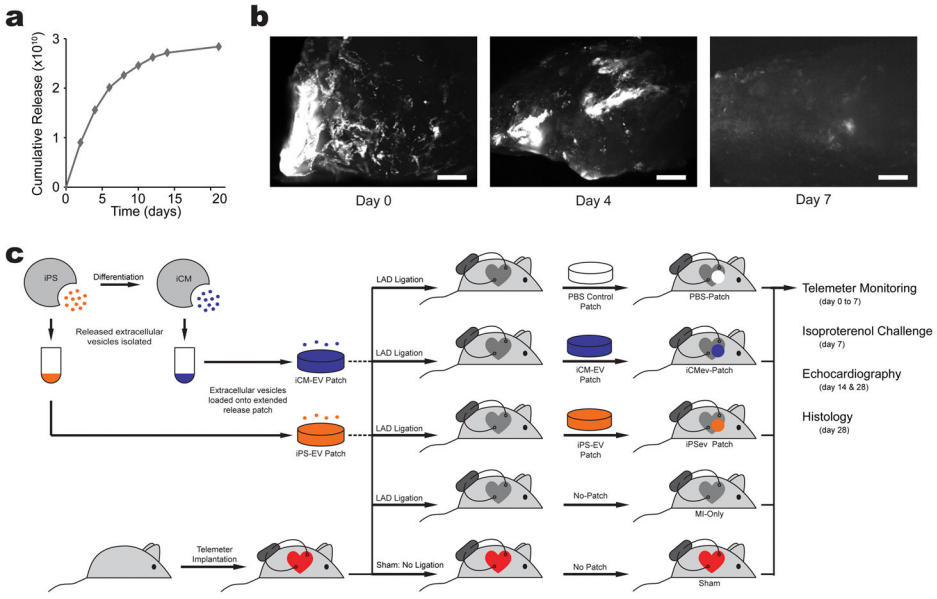

Figure 4. Hydrogel patch sustainably released encapsulated EVs in a rat heart infarction model

a) Cumulative release profile of EV-containing patches over 21 days in vitro as quantified by Nanosight (n = 2 biologically independent samples). b) Representative image of DiI stained EVs present in hydrogel patches explanted 0, 4, and 7 days after implant onto rat myocardium. (n = 1 biologically independent sample per day) (Scale bar 200uM) c) Schematic representation of the experimental set-up for the rat model: EVs are isolated from iPS cells or iCMs and incorporated into a patch as therapy in a rat acute myocardial infarction model.

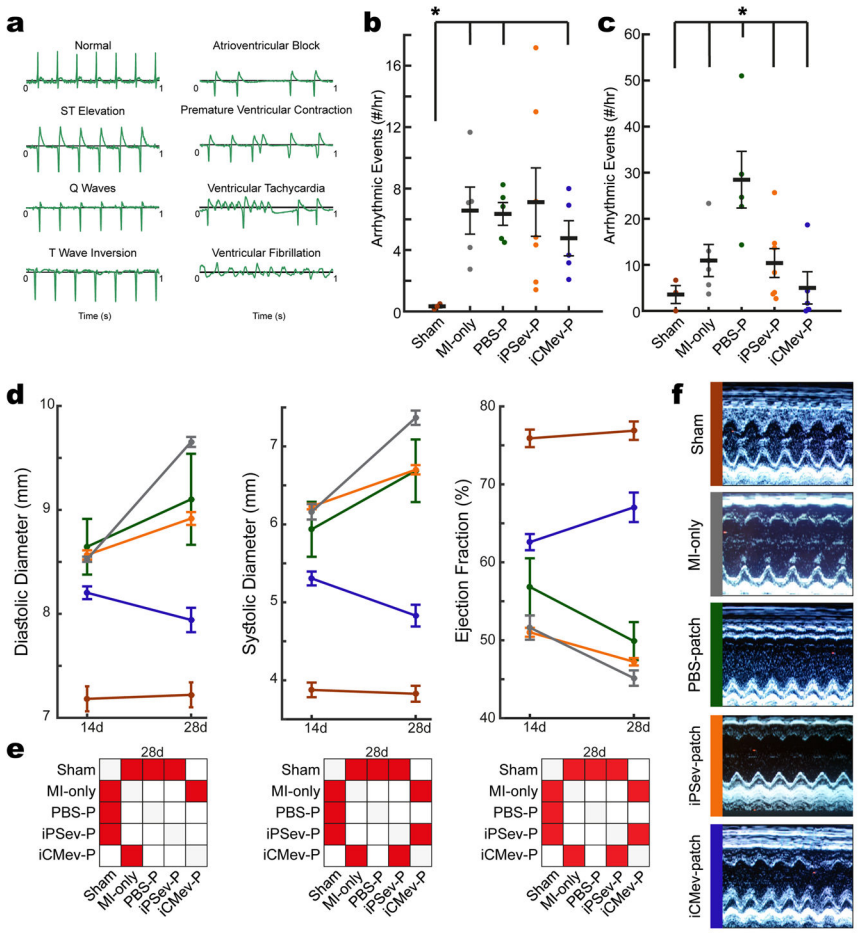

Figure 5. iCM-EVs are non-arrhythmogenic and promote recovery of heart contractile function

a) Electrocardiogram progression after LAD. All rats exhibited ST-elevations following LAD ligation, followed by Q waves and T-wave inversion within 3 days. LAD ligation resulted in arrhythmic events including atrioventricular block, characterized by a p-wave without a subsequent QRS complex, premature ventricular contraction, characterized by a widened QRS complex without a preceding p-wave, ventricular tachycardia, characterized by more than three consecutive QRS complexes without preceding p-waves, and ventricular fibrillation, characterized by uncoordinated electrical activity. b) Number of arrhythmic events per hour experienced by animals during the first 5 days after infarction (Average ± SEM, n = 3, 5, 5, 7, and 6 biologically independent samples for sham, MI-only, PBS-P, iPSev-P, and iCMev-P groups respectively)(* denotes $p<0.05$ by two sided T-test). c) Number of arrhythmic events per hour experienced by animals for 3 hours after isoproterenol challenge (Average ± SEM, n = 3, 5, 5, 7, and 5 biologically independent samples for sham, MI-only, PBS-P, iPSev-P, and iCMev-P groups respectively)(* denotes $p<0.05$ by two sided T-test). d) Quantified echocardiogram parameters of animals at 2 and 4-week time points. (Average ± SEM, n = 5, 4, 6, 7, 6 biologically independent samples for sham, MI-only, PBS-P, iPSev-P, and iCMev-P groups respectively). e) Statistical significance of quantified echocardiogram parameters between all groups at 4 weeks quantified by two tailed T-test. Red indicates a significant difference with Bonferroni

corrected $p < 0.05$. f) Representative M-mode echocardiographs at 4 weeks (experiments were repeated in n = 6, 5, 6, 7, and 6 animals for sham, MI-only, PBS-P, iPSev-P, and iCMev-P groups respectively with similar results).

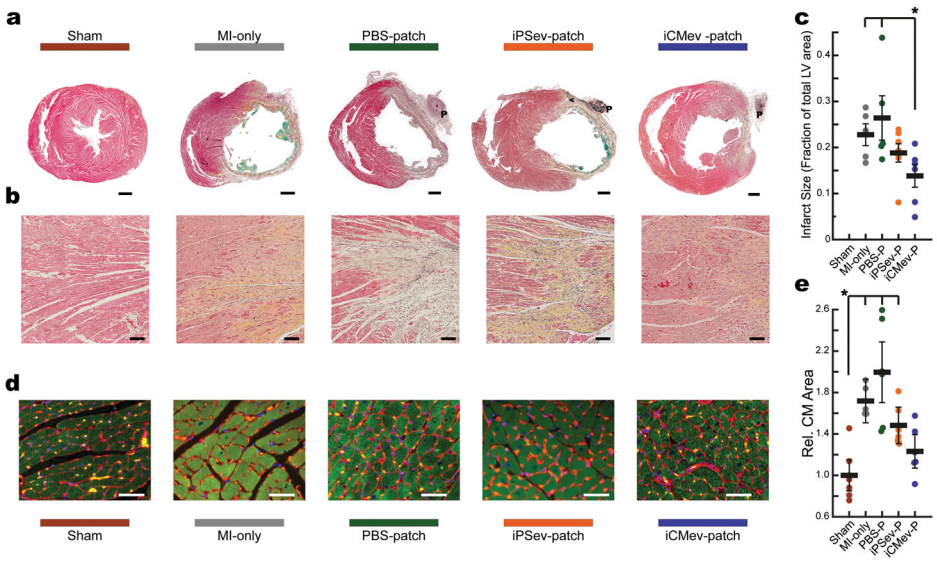

Figure 6. iCM-EV treatment reduced infarct size and CM hypertrophy

a) Representative transverse cardiac sections stained with Movat's pentachrome stain (scale bars = 1 mm). The letter P indicates the location of the patch. b) High power image of the infarct border zone (scale bars = 100 μm) (experiments were repeated in n = 5, 5, 7, 6 biologically independent samples for MI-only, PBS-P, iPSev-P, and iCMev-P groups respectively with similar results). c) Infarct size as a percentage of the total left ventricle (Average ± SEM, n = 5, 5, 7, 6 biologically independent samples for MI-only, PBS-P, iPSev-P, and iCMev-P groups respectively, * denotes $p < 0.05$ by two-tailed T-test). d) Sections were stained for wheat germ agglutinin (red), troponin (green), and DAPI (blue), and e) relative cardiomyocyte area was quantified. Scale bars = 50 μm. (Average ± SEM, n = 6, 5, 6, 6, and 6 biologically independent samples for sham, MI-only, PBS-P, iPSev-P, and iCMev-P groups respectively with similar results, * denotes $p < 0.05$ by two-tailed T-test).

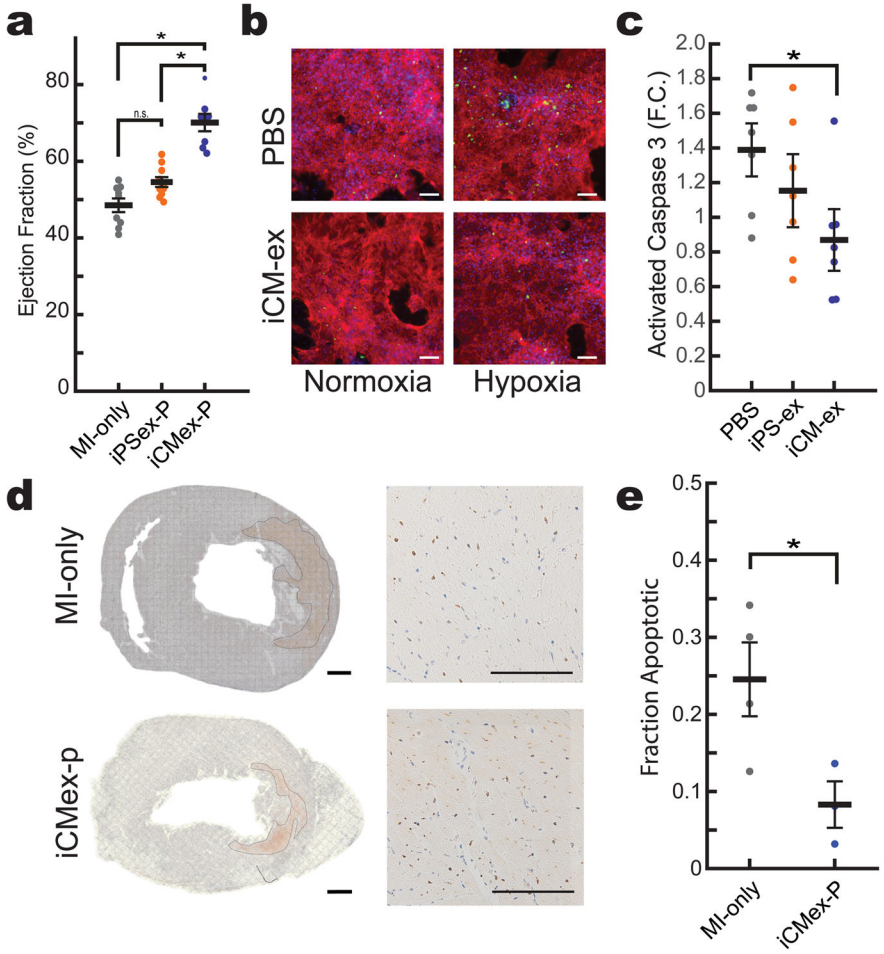

Figure 7. iCM-EV treatment prevents apoptosis in the acutely infarcted heart

a) Quantification of ejection fraction 24 hours after LAD ligation (Average± SEM, n = 9, 10, and 8 biologically independent samples for MI-only, iPSev-P, iCMev-P groups respectively, * denotes $p < 0.05$ by two-tailed T-test) b) Activated caspase 3 (green), troponin (red), and DAPI (blue) stained cardiomyocytes treated with iCM-EVs or PBS and subjected to hypoxia (scale bars = 100 um) c) Quantification of the numbers of caspase 3 positive hypoxic cardiomyocytes relative to normoxic cardiomyocytes (F.C. denotes fold change, Average± SEM, n = 7 biologically independent samples per group, * denotes $p < 0.05$ by two-tailed T-test). d) Representative transverse cardiac sections stained with TUNEL (scale = 1 mm) at high magnification (scale bars = 100um) e) Quantification of apoptotic area as a fraction of total left ventricular area. (Average ± SEM, n = 4 and 3 biologically independent samples for MI-only and iCMev-P groups respectively, * denotes $p<0.05$ by two-tailed T-test).

Table 1

miR	log fold change	iPS-EV (TPM)	iCM-EV (TPM)
hsa-miR-1	7.38	590	137765
hsa-miR-302a-5p	−2.52	371799	81598
hsa-miR-122-5p	7.92	49	75250
hsa-miR-92a-3p	−1.60	56168	24093
hsa-miR-143-3p	5.89	213	18692
hsa-miR-302b-3p	−3.31	146633	18151
hsa-miR-30d-5p	1.11	5538	15753
hsa-miR-27b-3p	2.42	1819	12754
hsa-miR-99b-5p	1.47	2940	10924
hsa-miR-200b-3p	1.75	2134	9108